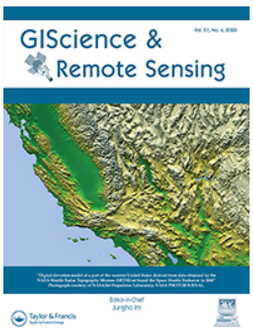

GIScience & Remote Sensing

ISSN: 1548-1603 (Print) 1943-7226 (Online) Journal homepage: https://www.tandfonline.com/loi/tgrs20

Deep learning-based water quality estimation and anomaly detection using Landsat-8/Sentinel-2 virtual constellation and cloud computing

Kyle T. Peterson, Vasit Sagan & John J. Sloan

To cite this article: Kyle T. Peterson, Vasit Sagan & John J. Sloan (2020) Deep learning-based water quality estimation and anomaly detection using Landsat-8/Sentinel-2 virtual constellation and cloud computing, GIScience & Remote Sensing, 57:4, 510-525, DOI: 10.1080/15481603.2020.1738061

To link to this article: https://doi.org/10.1080/15481603.2020.1738061

GISCIENCE & REMOTE SENSING
2020, VOL. 57, NO. 4, 510–525
https://doi.org/10.1080/15481603.2020.1738061

Taylor & Francis
Taylor & Francis Group

Deep learning-based water quality estimation and anomaly detection using Landsat-8/Sentinel-2 virtual constellation and cloud computing

Kyle T. Peterson[a], Vasit Sagan[a,b] and John J. Sloan[c]

[a]Department of Earth and Atmospheric Sciences, Saint Louis University, Saint Louis, MO, USA; [b]Geospatial Institute, Saint Louis University, Saint Louis, MO, USA; [c]National Great Rivers Research and Education Center, East Alton, IL, USA

ABSTRACT

Monitoring of inland water quality is of significant importance due to the increase in water quality related issues, especially within the Midwestern United States. Traditional monitoring techniques, although highly accurate, are vastly insufficient in terms of spatial and temporal coverage. Using a virtual constellation by harmonizing Landsat-8 and Sentinel-2 data a high temporal frequency dataset can be created at a relatively fine spatial scale. In this study, we apply a novel deep learning method for the estimation of blue-green algae (BGA), chlorophyll-α (Chl), fluorescent dissolved organic matter (fDOM), dissolved oxygen (DO), specific conductance (SC), and turbidity. The developed model is evaluated against previously studied machine learning methods and found to outperform multiple linear regression (MLR), support vector machine regression (SVR), and extreme learning machine regression (ELR) generating R^2 of 0.91 for BGA, 0.88, 0.89, 0.93, 0.87, and 0.84 for Chl, DO, SC, and turbidity respectfully. This model is then applied to all available data ranging from 2013–2018 and time series for each variable were generated for four selected waterbodies. We then use the Empirical Data Analytics (EDA) anomaly detection method on the time series to identify abnormal data points. Upon further analysis, the EDA method successfully identifies abnormal events in water quality. Our results also demonstrate strong correlation between non-optically active variables such as SC with Chl and fDOM. The framework developed in this study represents an efficient and accurate empirical method for inland water quality monitoring at the regional scale.

ARTICLE HISTORY
Received 1 September 2019
Accepted 28 February 2020

KEYWORDS
Deep learning; water quality; virtual constellation; anomaly detection

1. Introduction

Traditional monitoring and assessment of water quality has relied on in situ measurements, sample collection, and lab analyses to measure indicators related to the physical, chemical, and biological properties of the waterbody. More recently, federal agencies like the United States Geological Survey (USGS) and United States Environmental Protection Agency (USEPA), along with other partners are developing networks of sensors that provide continuous water quality data in near real-time (Pellerin et al. 2016). In situ methods such as those outlined in the USGS water quality sampling guide (Wilde et al. 2014), which are generally very accurate, are nevertheless quite time consuming, expensive, and provide point based data that lacks spatial and temporal detail and coverage (Duan et al. 2013). Due to these limitations, traditional in situ-based monitoring methods lack overall representativeness for inland water systems. To overcome issues related to spatial and temporal coverage remote sensing has been recognized as an ideal solution leveraging the capabilities of recent sensor and methodology improvements. The use of satellite remote sensing platforms allows for the monitoring and investigation of water quality at the regional and global scales. Remote sensing techniques allow for water quality and ecosystem health to be inferred via indicator variables such as blue-green algae (BGA), chlorophyll (Chl), fluorescent dissolved organic matter (fDOM), and turbidity that represent the biological and hydrological conditions of the waterbody (Gholizadeh, Melesse, and Reddi 2016).

Providing relatively fine spatial resolution and comparable spectral resolutions the Landsat-8 and Sentinel-2 multispectral satellites provide an opportunity for the development of a unique virtual constellation via multi-senor data fusion. Both platforms contain overlapping coastal, blue, green, red, near-infrared (NIR), and two shortwave-infrared (SWIR) bands making both Landsat-8 and Sentinel-2 capable of monitoring a range of water quality constituents (Pahlevan et al. 2014). Fusing these two satellite-based datasets would enable high-frequency revisit times of about three days (Li and Roy 2017) within the mid-latitudes. The exploratory study recently published by Pahlevan et al. (2019), displayed that the union of Landsat-8 and Sentinel-2 data to create

CONTACT Vasit Sagan vasit.sagan@slu.edu

a harmonized product is feasible and can be applied to water quality remote sensing investigations. This harmonized multispectral dataset would allow for nearly continuous monitoring of inland waterbodies and provide crucial information for water resource managers, limnologists, hydrologists, and aquatic ecologists. The enhanced revisit time provided through the harmonization of Landsat-8 and Sentinel-2 is crucial for water quality monitoring and assessment as inland water conditions can vary greatly over a short time period.

Recent studies have shown the efficacy of multispectral satellites including Landsat-8 and Sentinel-2 data for water quality variable estimation. Kutser et al. (2016) displayed the ability of Sentinel-2 data to quantitively estimate concentrations of Chl, total suspended matter (TSM), and suspended particulate organic matter with a relative degree of success utilizing a peak height algorithm at 705 nm and 783 nm. Toming et al. (2016), also exhibited the ability of Sentinel-2 for estimating Chl, chromophoric dissolved organic matter (CDOM), dissolved organic carbon (DOC), and turbidity using a similar spectral peak method. Several other studies have also utilized band ratio algorithms for estimating various lake water characteristics ranging from Chl, CDOM, and suspended matter to water turbidity using Landsat-8 (Lim and Choi 2015; Urbanski et al. 2016). Variables such as BGA, Chl, CDOM, and others representing the optically active constituents of inland water have been well explored by researchers, yet variables such as dissolved oxygen (DO) and specific conductance (SC) that are non-optically active have not. Being non-optically active, DO and SC estimation represent a distinct challenge to remote sensing (Dörnhöfer and Oppelt 2016; Schaeffer et al. 2013). To address this fundamental issue, indirect estimation of DO and SC through other indicator variables may serve as a viable solution.

To create better models, more sophisticated empirical approaches using neural networks (Odermatt et al. 2012) and physics-based inversion methods have recently gained some popularity among researchers. Some neural network-based approaches (Doerffer and Schiller 2007; Doerffer 2008), have shown promising results using MERIS data, proving to be transferable to some lakes and waterbodies with similar optical properties. Although much work has focused on water quality variable estimation, nearly all studies fail to achieve high accuracy and are site specific often applying to a single body of water. Although machine learning has shown promise to overcome these issues, the interactions between water constituents and solar radiation are quite complex and present a challenge for the typical machine learning approach. Deep learning methods however learn higher-order statistical relationships (Robert 2014), thus often outperforming traditional estimation and modeling approaches. Due to the unique challenges presented in water quality modeling, special attention should be applied to the model development. Here we propose a custom deep learning model architecture, progressively decreasing deep neural network (pDNN), designed specifically for satellite-based water quality modeling.

By incorporating the use of a Landsat-8/Sentinel-2 virtual constellation and deep learning regression methods for the estimation of key water quality variables we aim to establish a highly accurate and cutting-edge method for monitoring inland water quality at relatively high temporal resolutions. To create a deployable and highly efficient methodology, recent advances in cloud computing such as Google Earth Engine (GEE) and Google cloud are employed. The cloud computing based GEE is a free and immensely powerful tool for processing satellite data at a global scale.

Water quality problems are associated with several environmental and anthropogenic factors that are complex in nature, making prediction of impending outbreaks difficult. In addition to estimating the amount of water quality indicators, detecting changes and anomalies in these variables compared to long term average (e.g., sudden spikes, decreases, or abnormal levels of critical water quality variables) and historic outbreaks provides higher confidence in predicting water quality issues. Anomaly detection in this study is utilized and applied to all variables to serve as a water quality monitoring system and thus capture trends related to a range of biophysical properties. By incorporating an anomaly detection system for a range of water quality variables, distinct changes from the temporal and seasonal means can be identified. In this study, we look to extend what has been explored by previous studies by developing a cloud computing based regional water quality monitoring and anomaly detection platform by incorporating the harmonized Landsat-8 and Sentinel-2 dataset, deep learning, and cloud computing.

2. Materials and Methods

2.1. Study Area

The study area (Figure 1.) for this research focuses on several waterbodies contained within the Midwestern United States.

Sampling locations for ground-based water quality observations were located along two stretches of the upper Mississippi River in Wisconsin and two lakes located in central Illinois to obtain a range of hydrologic and atmospheric conditions across a regional scale. The

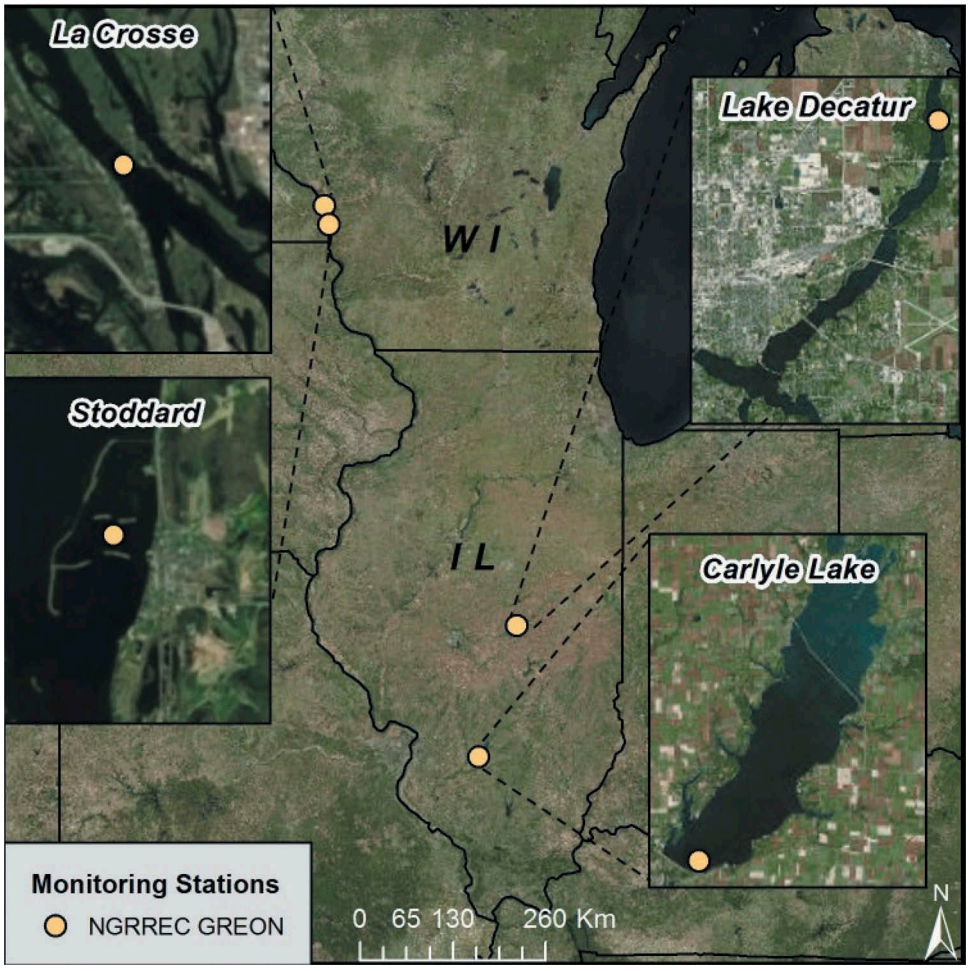

Figure 1. Map of the study locations displaying the selected waterbodies and the corresponding Great Rivers Ecological Observation Network (GREON) monitoring locations. (Refer to online version for colors)

two sampling locations located along the Mississippi River were located near La Crosse and Stoddard, Wisconsin. The La Crosse Great Rivers Ecological Observation Network (GREON) buoy located along the upper Mississippi River is situated mid-stream and monitors flowing water near the middle of the stream channel. The Stoddard GREON unit deployed about 10 miles downstream of La Crosse is located in backwater and protected by jetties to the north and west. This creates slow-moving shallow waters that tend to exacerbate algal growth.

The two reservoirs located in Central Illinois included in this study were Lake Decatur and Carlyle Lake. Located along the Sangamon River, Lake Decatur's watershed encompasses an area of 2396 km^2 and is dominated by cultivated agriculture. Recently, Lake Decatur has experienced extensive issues related to siltation due to soil erosion and increased levels of nitrogen and phosphorus compounds due to agricultural runoff containing fertilizers and animal waste (Kohler, Sheehan, and Sweatman 1993). Carlyle Lake also located in central Illinois, is one of two large reservoirs along the Kaskaskia River and has a total surface area of 105 km^2 and mean depth of 3.4 m (Romano et al. 2009). Situated within the Kaskaskia watershed the surrounding area is predominantly agricultural land (67%), mainly composed of corn and soybean fields (Chiang et al. 2012). Due to the high impact of agricultural tillage and tile drainage in Central Illinois, both Lake Decatur and Carlyle Lake provide ideal conditions for algal growth and related issues due to an over-abundance of nitrogen and phosphorus combined with shallow depths, calm surface waters and warm temperatures (Pearce, Chambers, and Hasenmueller 2017).

2.2. Satellite Data

Using the Google Earth Engine (GEE) cloud computing platform, Landsat-8 and Sentinel-2 datasets were obtained and processed for the time period between April 2015 and October 2018. Cloud filtering and masking is first performed using the provided pixel quality

assurance (QA) bands to select only pixels containing cloud free water. A standard deviation filter (Pereira et al. 2018) is then applied to the imagery to filter out passing ships and/or the GREON units deployed within the study area. The resulting datasets containing Landsat-8 Level-1 T and Sentinel-2 Level-1 C data are used in this study to increase the temporal resolution and create a harmonized Landsat-8-Sentinel-2 multispectral dataset (described subsequently). This harmonized data product is based on the framework established by Claverie et al. (2018). The harmonized Landsat-8 and Sentinel-2 (HLS) project is a NASA initiative to produce a virtual constellation of surface reflectance data from the Landsat-8 and Sentinel-2 satellite platforms. With the HLS, a temporal revisit time of 3 days is achieved at a relatively fine spatial resolution of 30 m (Pahlevan et al. 2019).

The HLS methodology (Figure 2), beginning with Landsat-8 level 1-T (L1-T), is first atmospherically corrected following the Land Surface Reflectance Code (LaSRC) developed by Vermote et al. (2016). Sentinel-2 Level 1-C (L1-C) data is concurrently processed using the Sen2Cor methodology (Louis et al. 2016) to calculate surface reflectance. The data is then masked for values indicating clouds, adjacent shadow, and cloud shadow using the CFmask procedure adopted from (Zhu, Wang, and Woodcock 2015). This may introduce minor error as the final surface reflectance product can contain contributions from specular reflectance (glint) at the water surface. The Sentinel-2 data is then resampled to a 30 m spatial resolution and the two products are geographically registered. A bidirectional reflectance distribution function (BRDF) normalization is then applied to each dataset which is used to compensate for the anisotropic reflectance of the earth's surface which varies based on the solar zenith angle and the view angle of the target location. A bandpass adjustment is then used to account for small spectral differences within overlapping band regions (Claverie et al. 2018). The Landsat-8 bandpasses are used as reference, to which the Sentinel-2 spectral bands are adjusted using a linear fit defined by Claverie et al. (2018) between equivalent spectral bands.

The resulting data products S-30 MSI and L-30 OLI contain fully corrected surface reflectance values for the seven overlapping bands and are virtually identical in terms of spectral response and spatial resolution. This creates the potential for synergistic use of the two satellite data sources and unprecedented opportunities for timely and accurate observation of Earth status and dynamics (Claverie et al. 2018). A detailed description of the HLS processing methodology can be found in Claverie et al. (2017). HLS data used for the modeling process were further masked to extract only the areas surrounding the GREON monitoring stations. A sampling area representing a 90 × 90 m (3 x 3 pixel) region is created for each site and the mean reflectance values are calculated and used as input spectral data for the modeling process. These sampling areas were manually demarcated to diminish issues related to adjacency effects. The resulting HLS imagery database generated 84 total scenes for Carlyle Lake, 89 for Lake Decatur, 74 for La Crosse, and 61 for Stoddard ranging from 1 April

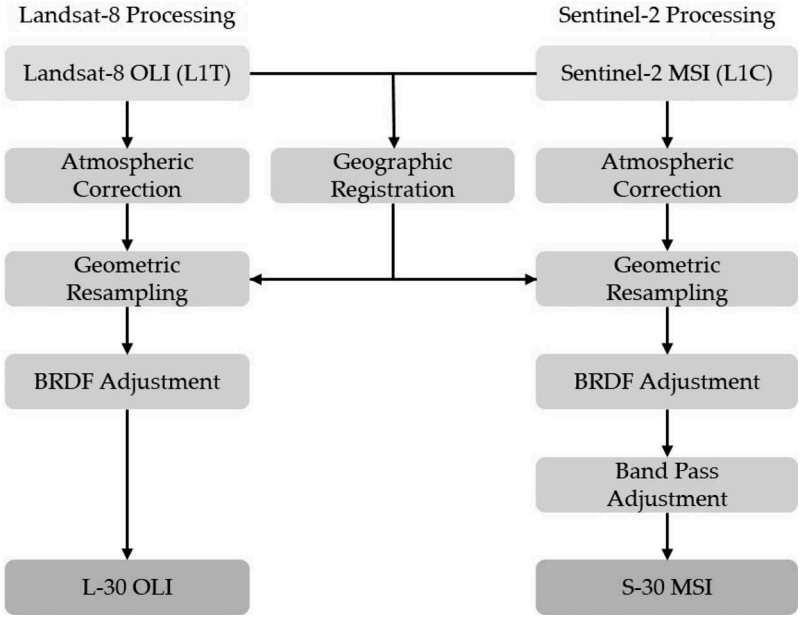

Figure 2. Satellite data preprocessing workflow as defined by the NASA HLS science algorithm. S-30 MSI and L-30 OLI represent the final harmonized data products at 30 m spatial resolution. Modified from Claverie et al. (2018). (Refer to online version for colors)

2013 to 18 October 2018. The resulting database of HLS imagery contained 244 scenes from Landsat-8 and 63 from Sentinel-2 (in operation since June 2015). The total number of scenes and temporal frequency of the dataset is limited due to cloud cover and atmospheric effects reducing the database by ~35%.

2.3. Water Quality Data

The water quality information used in this study was obtained and provided by the National Great Rivers Research and Education Center (NGRREC). Developed by NGRREC in 2013 the Great Rivers Ecological Observation Network (GREON) was established as a system of real-time water quality monitoring platforms within the Midwest and the Mississippi River watershed. In collaboration with YSI Inc. the GREON units (Figure 3) are designed to continuously monitor water quality using state-of-the-art sensor technology mounted on a floating platform providing a suite of water quality and weather-related parameters including water temperature, specific conductivity (SC), dissolved oxygen (DO), turbidity, chlorophyll (Chl), blue-green algae (BGA) biomass, and fluorescent dissolved organic matter (fDOM) representing the fraction of CDOM that fluoresces. Although this sensor provides a wealth of continuous data the units used for fDOM (QSU) and turbidity (FNU) are different from those used in standard laboratory tests. Thus, making a direct comparison of satellite-based results derived from GREON calibration data with other ground-based data is difficult.

The four selected GREON units used in this study provided in situ data from April 2013 to October 2018. Data corresponding to the overpass dates of the HLS imagery were parsed and assembled into the pairwise reflectance-water quality database. This generated a total of 97 days of corresponding reflectance-water quality pairs. Displayed in Table 1. are the summary statistics of the water quality data used in this study. All data obtained from the GREON network is publicly available and free of charge via the Great Lakes to Gulf (GLTG^{SM}) Virtual Observatory (https://greatlakestogulf.org).

With the use of multisensor data fusion we were able to produce and utilize a harmonized data product for Landsat-8 and Sentinel-2 leading to a significant increase in temporal resolution for the given study locations. Utilizing the HLS dataset, imagery for a total of 307 cloud free scenes were generated for the areas of interest assembling 244 scenes from Landsat-8 and 63 from Sentinel-2. Extending the temporal range of the study from 2013 to 2018 generated a much higher number of scenes for Landsat-8 than Sentinel-2, which was not launched until June 2015. The filtering process intended to remove cloud cover and select out water only pixels also lead to the lower number of total scenes and remains an inherent limitation of optical satellite remote sensing. Although these issues limited the total number of scenes and temporal resolution of the HLS dataset, it still displayed improvement over the use of a single sensor by significantly improving the revisit time. Increasing the revisit time via multisensor data fusion, an improved monitoring capability is enabled and can help to further our knowledge of water quality dynamics for inland areas.

2.4. Water Quality Modeling

The water quality modeling process is conducted in several stages beginning with the assemblage of the water quality-reflectance dataset. Utilizing this data, a

Figure 3. Images of the NGRREC GREON field monitoring buoys. The GREON network is deployed in several waterbodies across the Midwestern United States and continuously gathers a range of water quality measurements. (Refer to online version for colors).

Table 1. Summary statistics of the water quality data used for the modeling process. *Two samples containing invalid SC measurements were removed reducing the SC database to 95 samples.

	BGA (ug/L)	Chl (mg/L)	DO (mg/L)	fDOM (QSU)	SC (uS/cm)	Turbidity (FNU)
n	97	97	97	97	95*	97
mean	2.2	17.4	6.0	64.3	419.4	16.8
min	0.1	0.6	0.1	0.3	247.9	2.0
max	9.3	74.4	19.7	156.2	654.8	131.1
Std. dev.	2.3	17.4	4.9	38.7	109.0	15.2
variance	5.1	301.1	23.5	1498.4	12,408.8	230.2

pairwise dataset containing overlapping in situ water quality measurements obtained from the GREON monitoring system and corresponding spectral reflectance information derived from the Landsat-8-Sentinel-2 virtual constellation is compiled. This dataset contained 97 samples representing 37 samples gathered from GREON locations along the Mississippi River, 28 from Carlyle Lake, and 32 from Lake Decatur. Two extraneous samples containing uncommonly low values were removed from the SC database which to prevent issues in the modeling process. Data is randomly partitioned 60% for training and 40% for testing.

2.4.1. Feature Extraction

To supplement the seven raw HLS spectral bands a series of additional spectral features are extracted to add key information based on standard band ratios (Dekker, Malthus, and Seyhan 1991; Doxoran, Froidefond, and Castaing 2003; Lathrop and Lillesand 1989; Odermatt et al. 2012; Ritchie, Zimba, and Everitt 2003; Sudheer, Chaubey, and Garg 2006; Svab et al. 2005) and the biophysical properties of the water quality constituents. Band arithmetic/ratios, such as those calculated, make use of known associations between a given water quality parameter and one or more spectral bands that are sensitive to the sought-after optical property. Displayed in Table 2. is the comprehensive list of spectral features created from the HLS dataset. This produces a total of 21 predictor features representing the spectral reflectance characteristics of the given sampling area.

2.4.2. Progressively decreasing deep neural network (pDNN)

A range of machine learning based regression methods and approaches are explored in this study for quantitatively estimating water quality variables from the HLS reflectance data. Traditional machine learning methods or "shallow" paradigms typically include limited processing stages that connect the input data to the prediction, e.g., data enhancement, feature extraction, and then regression. These methods including multiple linear regression (MLR),

Table 2. List of the spectral features derived from the HLS dataset.

Spectral Feature	Formula
Coastal	HLS Band 1
Blue	HLS Band 2
Green	HLS Band 3
Red	HLS Band 4
NIR	HLS Band 5
SWIR 1	HLS Band 6
SWIR 2	HLS Band 7
Ratio of Green and Red	Green/Red
Ratio of Green and Blue	Green/Blue
Ratio of Red and NIR	Red/NIR
Ratio of Red to blue	Red/Blue
Ratio of Red and Green	Red/Green
NGRDI	(Green-Red)/(Green+Red)
Normalized Difference Chlorophyll Index (NDCI)	(NIR-Red)/(NIR+Red)
Green plus Red divided by 2	Green+Red/2
Ratio of Red and Green plus NIR	Red/Green+NIR
Normalized difference NIR and SWIR 1	(NIR-SWIR 1)/(NIR+SWIR 1)
Normalized difference Green and NIR	(Green-NIR)/(Green+NIR)
Normalized difference SWIR 1 and SWIR 2	(SWIR 1-SWIR 2)/(SWIR 1-SWIR 2)
Normalized difference Green and SWIR 1	(Green-SWIR 1)/(Green+SWIR 1)

partial least squares regression (PLSR), and support vector machine regression (SVR), to name a few, have been widely employed for water quality-based studies and have been shown to accurately model low to mid-level relationships relatively well (Ryan and Ali 2016; Wang et al. 2017; Rokni et al. 2015). In contrast, deep learning models can contain many levels of processing layers that allow a rich variety of complex, non-linear, high-level relationships to be learned from the given data (Schmidhuber 2015). Deep learning is one of the fastest growing trends in a number of fields related to remote sensing and represents a major breakthrough for big data and remote sensing analysis (Van Der Woerd and Pasterkamp 2008; Zhang, Zhang, and Du 2016). Deep learning is fundamentally based on neural networks (NNs), which in their basic form consist of structures of fully connected neurons that apply a non-parametric function to the output of a linear regression problem.

One of the primary goals of this research is to assess the utility of deep learning in water quality remote sensing applications since no previous work to our knowledge has utilized this approach. The most commonly employed form of a NN is the feedforward model. In this supervised learning approach, information is passed forward along the network with no looping. First, information passes through the input nodes and then through a series of hidden nodes that take in a set of weighted inputs and produce an output through a specified activation function. The feedforward model uses a set of corresponding input pairs from the training dataset containing *N* input vectors, with the corresponding *N* output values (Hornik, Stinchcombe, and White 1989). In this study, we implement a fully connected deep feedforward neural

network containing a single input layer, six hidden layers with a progressively decreasing width (number of processing nodes), and a single output (regression) layer. In order to determine the model depth (number of hidden layers) and complexity (processing nodes) an adaptive learning approach is utilized which begins with a single hidden layer and single processing node. Through iteration the number nodes are exponentially increased along with the number of layers until there is no longer improvement. This network utilizes Bayesian regularization backpropagation (MacKay 1992) along with the mean squared normalized error (MSE) performance function to optimize model parameters and the hyperbolic tangent sigmoid activation function for each hidden layer. The overall architecture of the progressively decreasing deep neural network (pDNN) is displayed in Figure 4.

Traditional machine learning techniques such as MLR, SVR, and extreme learning machine regression (ELR) were also applied to the dataset to evaluate the results of the pDNN. These techniques were chosen to evaluate the developed deep network against both linear (MLR) and non-linear methods (SVR and ELR). MLR is a simplistic model that attempts to model the relationship between two or more explanatory variables and a response variable by fitting a linear equation to observed data (Andrews 1974). SVR is a popular machine learning method for regression, first identified by Vapnik (1995) and is considered a nonparametric technique because it relies on kernel functions. The SVR model utilized in this study employes a linear kernel function and used sequential minimal optimization (Schölkopf and Smola 2001) to solve the quadratic programming. To represent a cutting-edge shallow learning technique ELR is also tested. Like the pDNN, ELR is a feed-forward neural network but contains a single hidden layer. In the previous study by Peterson et al. (2018a) ELR was found to outperform PLSR, SVR, and other shallow NN architectures when applied to water quality variable estimation from satellite data. The ELR method automatically generates and updates weights of the hidden layer without iterative optimization leading to significantly less computational time and robust approximations (Huang, Zhu, and Siew 2006). Huang, Zhu, and Siew (2006) provide an in-depth description of the ELR method and its mathematical formulation. The results of the modeling techniques are assessed using the coefficient of determination (R^2), root mean square error (RMSE), and the mean absolute percentage error (MAPE). All regression modeling techniques conducted in this study are implemented on a local machine using the MATLAB 2018b standard library with exception to ELR that can be downloaded from http://www.ntu.edu.sg/home/egbhuang/elm_codes.html. Regression modeling and following analysis are conducted outside the GEE platform due to algorithmic limitations in the GEE provided library.

2.4.3. Anomaly Detection

The detection and identification of anomalous values in a dataset is an important aspect of real-world events and represents a deviation from normal or expected patterns. The ability to identify anomalous levels of water

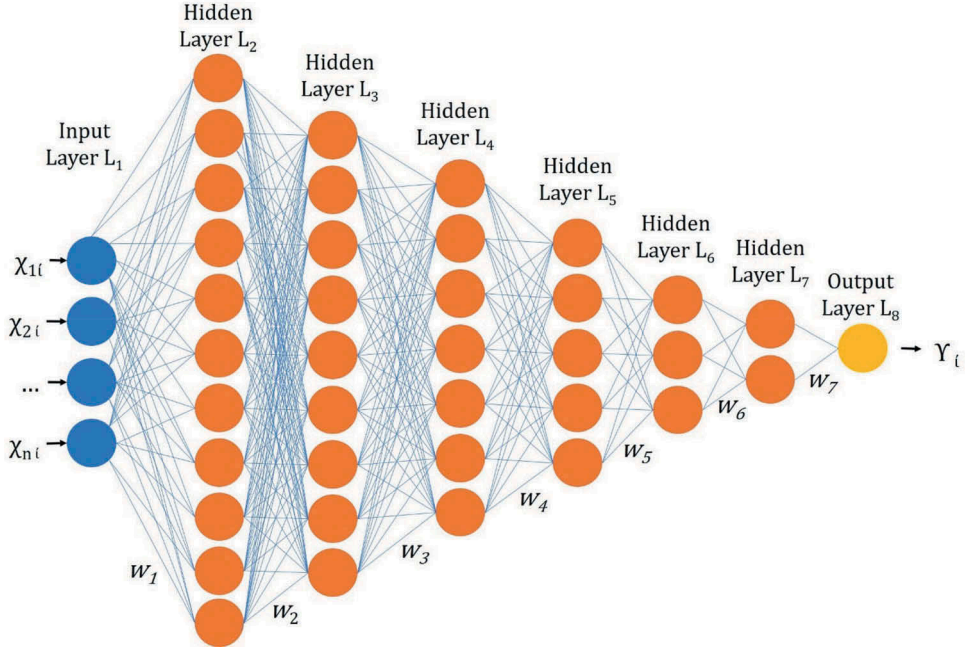

Figure 4. A visualized model representing the progressively decreasing deep neural network (pDNN). The pDNN takes a given input X_i representing the spectral features from the HLS dataset and is then fed into a series of six hidden layers and produces a final predictive output Y_i. In this diagram *w* represents the weight variable applied to the interconnections between the neurons. (Refer to online version for colors).

quality variables such as BGA, Chl, DO, fDOM, SC, and turbidity may increase the ability of decision-makers to respond to water quality issues and increase our understanding of inland hydrodynamics. Here we implement an autonomous anomaly detection method based on the Empirical Data Analytics (EDA) framework proposed by Angelov et al. (2016). The EDA based approach is a fully data-driven technique utilizing three non-parametric estimators: cumulative proximity, unimodal density, and multimodal density (Angelov et al. 2016; Gu and Angelov 2017) to identify potential anomalies. The cumulative proximity (Q) can be described as the square form of distance between points in a dataset (Angelov 2014). Cumulative proximity at x_i is expressed as:

$$Q(x_i) = \sum_{j=1}^{K} d^2(x_i, x_j), \tag{1}$$

where denotes the distance or dissimilarity between data points and while K signifies number of data points. Representing an indicator of the inverse of standardized eccentricity (Angelov et al. 2016), unimodal density (Q) is denoted as:

$$D_K(x_i) = \varepsilon_K^{-1}(x_i) = \frac{\sum_{j=1}^{K} qK(x_i)}{2K_{qK(x_i)}} = \frac{\sum_{j=1}^{K} d^2(x_j, x_k)}{2K\sum_{j=1}^{K} d^2(x_j, x_k)}, \tag{2}$$

where ≤ (Q) ≤ 1. Furthermore, the multimodal density (D^G) at a given data point u_i, is defined as the combination of the unimodal density weighted by the corresponding frequency of occurrence of the data point f_i. This is denoted as:

$$D_K^G(u_i) = f_i D_K(u_i) = f_i \frac{\sum_{j=1}^{K}\sum_{k=1}^{K} d^2(x_j, x_k)}{2K\sum_{j=1}^{K} d^2(x_j, x_k)}. \tag{3}$$

The multimodal density combines information regarding the frequencies of occurrence for each data point and their location in the given data space.

The use of these estimators reveals underlying trends and identifies anomalies based on the distribution and collective attributes of the given dataset along with taking the frequency of occurrences into consideration (Angelov et al. 2016). The EDA method is applied in two stages: (1) detecting potential anomalies using the estimators and (2) identifying local anomalies after forming possible data clouds (Angelov and Yager 2011) from the potential anomalies (Angelov et al. 2016). This approach has been compared to the "3σ" (Thomas and Balakrishnan 2009) and outlier detection using random walks (ODRW) (Moonesinghe and Tan 2006) methods and is proven to be a more accurate and objective method for anomaly detection while being equally effective at identifying both global and local anomalies (Angelov et al. 2016). The anomaly detection is performed on the downloaded data generated from the results of the regression modeling.

3. Results

3.1. Regression Modeling Results

The results of the regression modeling are displayed in Table 3. As expected, the models with the highest overall correlations and lowest RMSE and MAPE were generated by the pDNN method. The pDNN method proved to be quite robust generating R^2 values greater than 0.83 for all variables with a mean of 0.89 across the given water quality parameters when applied to the testing dataset. The pDNN method showed significant improvement over all other modeling techniques with ELR producing the second highest correlations with a mean testing R^2 of 0.78 across all variables. The pDNN method displayed a 13.28% mean increase over the ELR method, 27.63% over SVR, and 84.22% over MLR when evaluated using R^2 for the testing dataset. The SVR method showed slightly lower correlations than ELR models while MLR generated the lowest accuracies in all cases. By variable the best results were seen when estimating fDOM concentrations followed by BGA, DO, Chl, SC, and turbidity respectively. When evaluated by RMSE and MAPE the results mirrored the R^2 values proving the pDNN method superior to linear regression and traditional machine learning methods. The pDNN method also exhibited a low degree of overfitting with only slight differences between training and testing results. This is significant given the relatively small dataset ($n < 100$) which generally leads to overfitting issues as seen in the comparative methods (ELR, SVR, and MLR) evaluated in this study.

The plotted results of the pDNN models for each variable are displayed in Figure 5. Overall the models successfully predicted a range of variable concentrations. As shown by the results, models developed for DO, SC, and turbidity displayed more error predicting higher values. The BGA model, although highly accurate, also showed some error in estimating very low values that were present in the testing data. Overall, the models generated, accurately captured a range of high and low values across the testing dataset, especially Chl and fDOM, demonstrating that the pDNN method provides good generalization abilities and can be accurately utilized to estimate a range of water quality variables.

3.2. Anomaly Detection Results

The best overall model (pDNN) developed for each variable from the regression analysis is then applied to the

Table 3. Results of the regression modeling between HLS derived spectral features and the corresponding GREON monitoring station water quality data. Highlighted in bold are the best model results for each sensor when applied to testing dataset.

			BGA (ug/L)	Chl (mg/L)	DO (mg/L)	fDOM (QSU)	SC (uS/cm)	Turbidity (FNU)
MLR	Training	R^2	0.537	0.793	0.928	0.883	0.843	0.908
		RMSE	1.437	12.372	13.654	13.666	48.242	5.429
		MAPE	30.753	28.045	8.899	5.196	1.230	5.878
	Testing	R^2	0.338	0.499	0.440	0.651	0.563	0.398
		RMSE	1.986	7.912	3.309	21.951	62.296	7.169
		MAPE	33.492	32.467	13.976	6.098	1.789	22.598
SVR	Training	R^2	0.874	0.784	0.902	0.877	0.901	0.821
		RMSE	0.792	7.234	1.519	13.999	31.682	3.620
		MAPE	22.576	28.557	9.208	4.891	0.879	8.876
	Testing	R^2	0.701	0.584	0.805	0.656	0.744	0.679
		RMSE	1.298	11.906	2.141	21.799	31.682	5.897
		MAPE	28.223	31.489	12.265	6.278	1.267	14.556
ELR	Training	R^2	0.853	0.817	0.900	0.916	0.914	0.881
		RMSE	0.810	7.023	1.535	9.295	29.273	3.308
		MAPE	23.178	27.856	9.023	3.789	0.825	7.999
	Testing	R^2	0.804	0.694	0.818	0.824	0.728	0.829
		RMSE	1.080	10.283	2.070	19.136	66.566	8.586
		MAPE	24.864	29.814	11.298	5.677	1.343	11.857
DNN	Training	R^2	0.926	0.912	0.907	0.928	0.909	0.979
		RMSE	0.838	7.309	2.059	14.422	46.994	3.962
		MAPE	20.333	25.670	9.010	3.572	0.849	4.289
	Testing	R^2	**0.911**	**0.883**	**0.894**	**0.926**	**0.870**	**0.839**
		RMSE	**0.863**	**7.561**	**1.806**	**14.496**	**48.463**	**5.190**
		MAPE	**21.72**	**26.71**	**9.08**	**3.886**	**0.91**	**9.87**

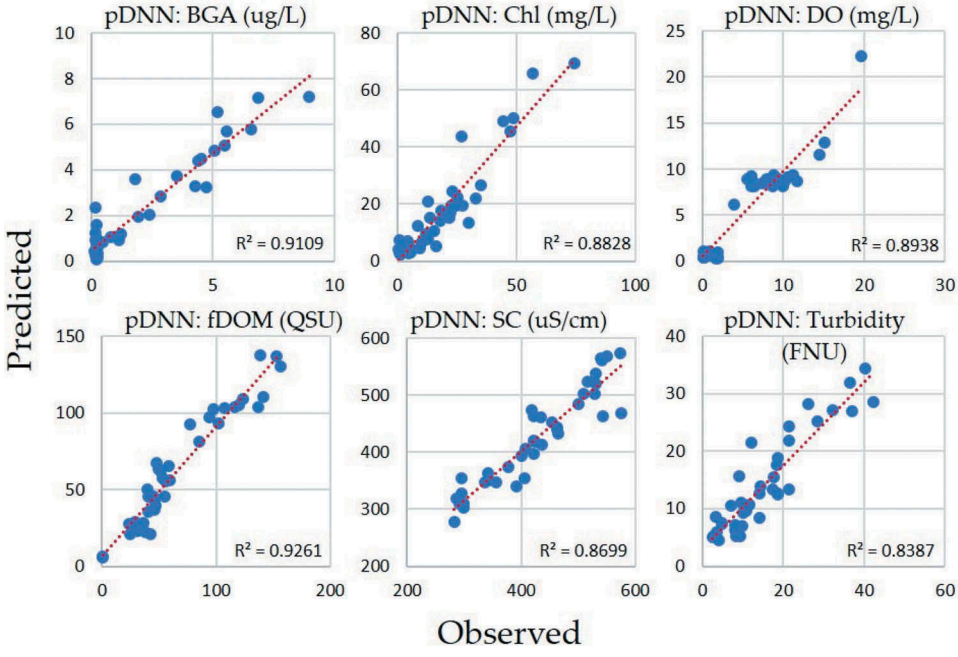

Figure 5. Plots of the observed versus predicted water quality values when applying the pDNN method to the testing dataset. (Refer to online version for colors).

entire HLS imagery dataset creating a time series of estimated water quality values for all four waterbodies located within the study area. Displayed in Figure 6. are the estimated water quality concentrations from 2013 to 2018 when applying the pDNN method to the entire HLS dataset for each location. Once the time series for each respective variable is generated, the EDA anomaly detection method is applied to each variable independently. Figure 6. shows the data points identified as anomalies highlighted in red along with the available ground truth data displayed in purple. The estimated values for most water quality variables aligned well with the observed ground truth data although limited. Values of BGA estimated for the La Crosse and Stoddard locations displayed some error as the model over predicted the majority of the observed data. This is likely due to the extremely low levels of observed BGA present in both locations which could prove difficult in modeling.

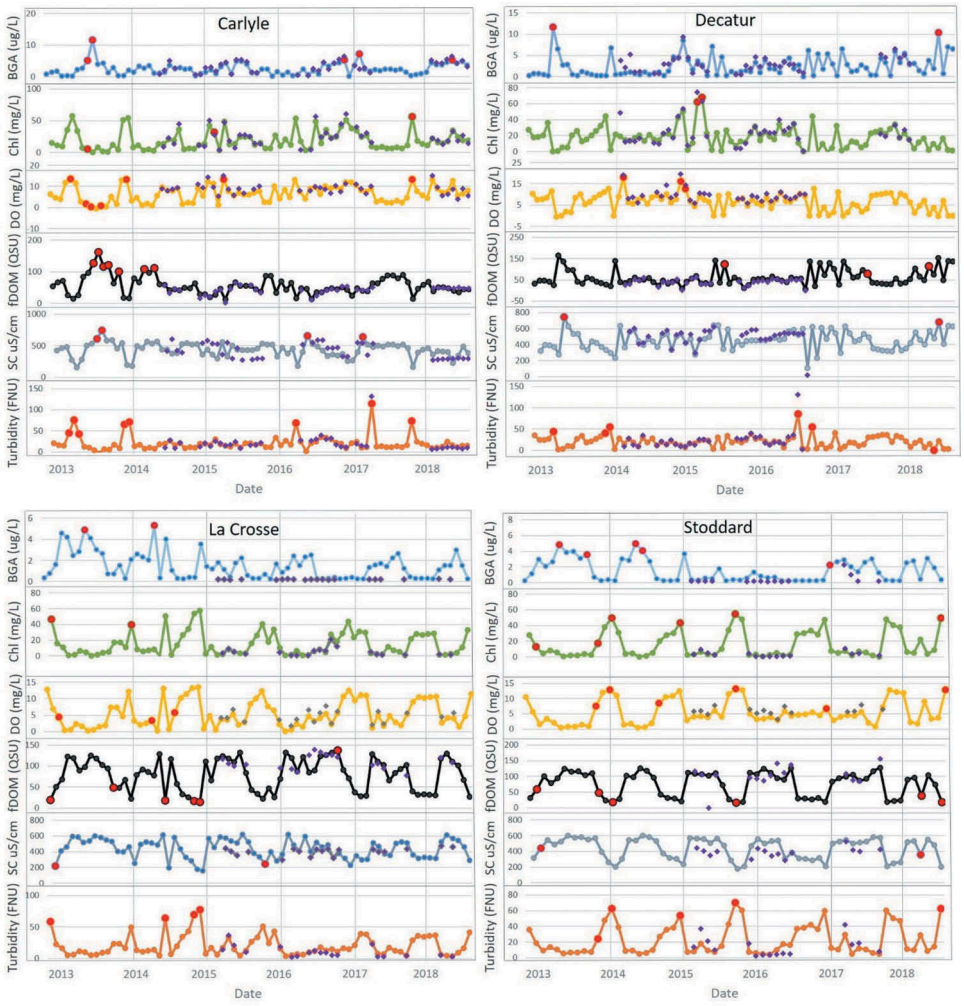

Figure 6. Time series of estimated water quality variables for the selected study areas. Estimated values are for the 90 m area surrounding the GREON monitoring station. The purple points indicate in situ-based measurements recorded by the GREON station. Data points that were identified as anomalous are highlighted by the red circles. (Refer to online version for colors).

Examination of the anomaly detection results displayed seasonal trends and similar timing of anomalies were found across locations. Most the identified anomalies occurred within the period between April and October for all variables. Trends in BGA showed anomalies occurred most frequently in the month of August containing six of the fourteen anomalies. The seasonal trends displayed for fDOM tended to follow BGA while identified anomalies coincided a limited number of times. Results generated for Chl and DO were very similar in all cases and followed a similar temporal trend. As seen in the results for Carlyle, Decatur, and Stoddard trends in both the temporal dynamics of Chl and DO along with time series anomalies generally aligned. The estimated time series for SC closely mirrored those produced for BGA and fDOM (Figure 7) also producing similar temporal trends in anomalies.

Finally, turbidity anomalies and its temporal trends displayed mixed results appearing to have some correlation to BGA, Chl, and DO while having an inverse relationship to fDOM and SC in nearly all cases.

To showcase the quantitative water quality estimation method generated in this study several HLS scenes that coincided with identified anomalies were selected to exhibit the spatial trends and continuous data that can be produced using this approach. One scene for each area of interest was selected based on the results of the anomaly detection process. Figure 8(a) is the estimated water quality for Carlyle Lake, IL on 15 September 2017 where anomalous levels of both BGA and SC were detected. HLS scenes were also selected for Lake Decatur on 4 October 2018 due to BGA and SC anomalies (Figure 8(b)) and La Crosse on 4 August 2014 for anomalous BGA levels (Figure 8(c)). The final scene selected was for the Stoddard location (Figure 8(d)) on 25 March 2016 where Chl, DO, and turbidity were all identified as anomalies. Applying the trained pDNN

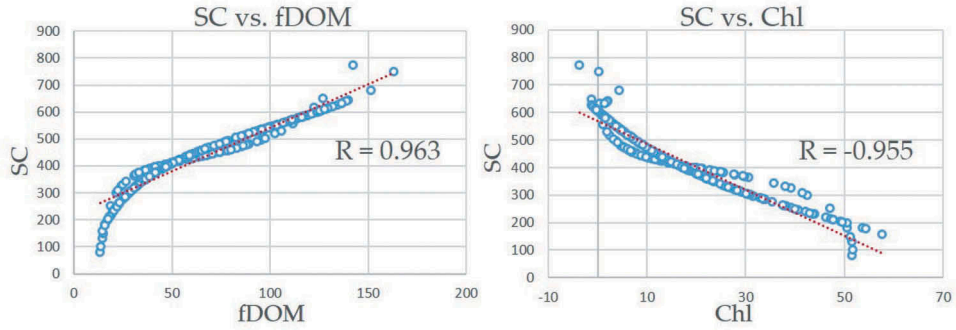

Figure 7. Plotted results of the water quality variable estimates over the 2013–2018 time period. Data from all locations were included in the analysis. The plotted results indicate a strong linear relationship between SC, fDOM, and Chl. (Refer to online version for colors).

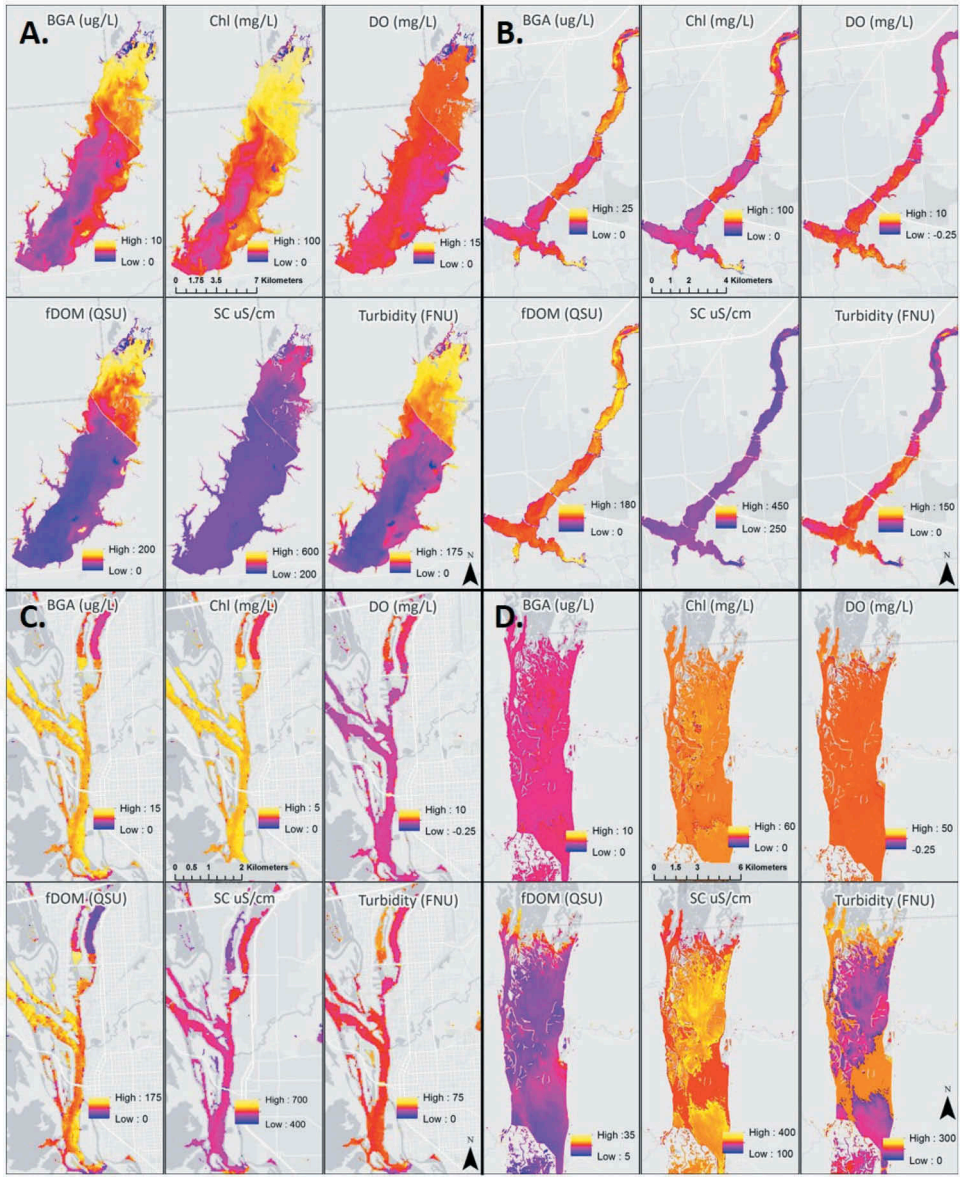

Figure 8. Maps of the estimated water quality parameters for Carlyle Lake (a) on 15 September 2017, Lake Decatur (b) on 4 October 2018, La Crosse (c) on 4 August 2014, and Stoddard (d) on 25 March 2016. (Refer to online version for colors).

model for each variable to the selected scenes produced the maps displayed in Figure 8.

Given the 30 m spatial resolution of the HLS data, detailed patterns in hydrological conditions are made clear and spatial patterns can be visually identified. On brief inspection of the water quality maps, it is clear that given the broad spatial extent (i.e. Carlyle, Decatur, and La Crosse) distinct differences can found based on the location. For example, in Figure 8(a). there is a noticeable difference in nearly all variables between the northern and southern portions of Carlyle Lake. This similar pattern is present throughout the selected scenes. For example, this is also apparent in Lake Decatur (Figure 8(b)) where the northern and southern reaches of the lake show significant differences and for La Crosse and Stoddard where manmade barriers within the river create clear differences in water quality trends. The spatial distribution of water quality variables further supports the findings and trends identified during the anomaly detection analysis. Maps such as these support the idea that remote sensing derived information can provide improved insight into the dynamic temporal and spatial trends in bio-hydrochemical concentrations, especially when compared to traditional in situ-based approaches.

4. Discussion

Employing the fused HLS dataset, a novel deep learning approach was tested for the prediction of water quality variables across the given study locations. The pDNN method proved to be quite robust generating highly accurate models for BGA with a R^2 = 0.91, Chl = 0.88, DO = 0.89, fDOM = 0.93, SC = 0.87, and turbidity = 0.84. The results from the pDNN method showed vast improvements over linear regression (MLR) and traditional (shallow) machine learning techniques (Table 3). This trend that has been seen over the last several years as regression methods based on machine learning techniques (e.g., SVR, ELR, neural networks), and more recently deep learning, have become attractive due to their robustness in a range of applications (Lary et al. 2016; Zhang, Zhang, and Du 2016; Zhu et al. 2017). Previous studies related to the prediction of water quality in inland areas (Peterson et al. 2018a, 2018b) have generated similar results proving that higher-level nonlinear methods and data representations may be better suited to model the complex relationships between water constituents and spectral reflectance. Taking a deep learning approach to modeling water quality enables a nested set of higher order relationships (exponentially higher given the number of hidden layers) to be extracted from the given dataset.

It is likely that these higher-level relationships enable non-optically active variables such as DO and SC to be predicted with high accuracy in this study. Using the extracted spectral features to supplement the HLS bands (Table 2) both low (band ratios and initial processing layers) and high order (resulting from the last processing layers of pDNN) relationships can be learned using the pDNN method. The results support the hypothesis that a series of complex relationships exist between non-optically and optically active variables. For example, the MLR method generated R^2 values of 0.44 and 0.56 for DO and SC, while pDNN resulted in R^2 values of 0.89 and 0.87 for DO and SC respectively. Although deep learning methods may overcome issues related to modeling the water constituent-reflectance relationship the underlying bio-physical interactions are not fully illuminated. The interpretability of model results is one of the main issues regarding the use of some machine learning and deep learning methods in particular (Lipton 2016). The use of a priori feature extraction, as in this study, may help to limit the scope and mystery of model interoperability by selecting input features based on expert knowledge (Schmidhuber 2015).

The pDNN method also displayed good generalization ability when applied to a range of variable concentrations after being trained on a limited dataset (n < 100). The testing dataset also contained samples from all four locations, thus performing well on all waterbodies addressed in this context. As seen in Figure 5, models for Chl and fDOM appeared to have the best generalization ability accurately predicting high and low values. The models developed for DO, SC, and turbidity had some minor difficulty predicting values in the higher ranges. Although highly accurate, the BGA model also showed some error in estimating very low values that were present in the testing data. These errors in prediction are likely due to the limited size of the training dataset used within this study and may have been skewed by the data partitioning and temporal availability of in situ water quality measurements. This is seen in the case of BGA, where a high amount of very low values was present in the testing data. The overall strength of the model's generalization ability is likely due to the use of four independent study areas across the Midwest. The water quality data acquired in this study was selected from both fluvial and reservoir environments over the course of several years providing a robust picture of regional water quality trends. Although this model performed well on the tested study areas it may not be applicable in other regions where hydrologic and atmospheric conditions differ. Transferability to other waterbodies outside of the study was not addressed herein but would be beneficial in future research.

In addition to the generalizability of the pDNN approach there was also noticeably lower overfitting when compared to the other methods. The degree of overfitting can often be related to a very high number of trainable parameters within the network. Several steps were taken in the design of the pDNN architecture to reduce issues of overfitting including limiting the number of processing nodes within each hidden layer, utilizing early stopping during model training, and the use of regularization in the backpropagation paradigm which has been proven to reduce model overfitting (Nielsen 2015). Data was also randomly partitioned 60% for training and 40% testing to further avoid related issues given the comparatively smaller sample size. Therefore, results of this study prove deep learning methods, within a similar context, may serve as improved modeling approaches especially when applied to variables that are difficult to model and contain a low signal-to-noise ratio (Kang, Min, and Ye 2017).

Applying the developed model to the HLS dataset, time series for estimated water quality concentrations at each location were generated from 2013–2018 (Figure 6). With the results of the estimated water quality concentrations across time the EDA anomaly detection method was applied and identified anomalous values for each variable. The EDA method is a fully data-driven (unsupervised) method and is free from user defined thresholds. In the case of water quality, where variable thresholds differ by region or have not been explicitly defined an unsupervised method such as EDA is ideal. This approach represents a more objective method for anomaly detection and is not only based on the global mean of the dataset but includes the idea of cumulative proximity, unimodal density, and multimodal density. The EDA method also incorporates the mutual distribution of the data within the data space along with the frequencies of occurrences into consideration. Thus, the EDA method has been found superior to many other unsupervised techniques and is highly computationally efficient (Angelov et al. 2016; Gu and Angelov 2017).

The generated time series displayed seasonal trends and similar timing among anomalies across locations. A large majority of the anomalies that were identified occurred between the months of April and October. Furthermore, the most noticeable trend in the time series data was the reoccurrence of BGA anomalies in the month of August. As is well known from previous literature, BGA tends to see the largest growth during summer months due to warmer water temperatures, calm surface conditions, and higher concentrations of N and P compounds resulting from agricultural application and runoff (Reavie et al. 2014). The time series data also revealed that fDOM tended to follow a similar pattern to BGA. This indicates that the phycocyanin pigment measured at 590 and 685 nm and the non-photosynthetic organic matter measured by fDOM at 480 nm were correlated. Trends and anomalies for Chl and DO also appeared to align, which is supported by other research that found Chl and DO correlated because DO is a product of photosynthesizing algae (Wallace, Champagne, and Hall 2016). Time series and anomalies generated for SC in most cases mirrored Chl and fDOM patterns. Figure 7 shows the strong linear relationship between SC and fDOM along with SC and Chl. These relationships displayed between SC, fDOM, and Chl further support the idea that SC is likely indirectly estimated via optical constituents. Lastly, turbidity displayed mixed results demonstrating loose relationships to Chl and an inverse relationship with BGA, fDOM, and SC. Depending on the levels of inorganic and organic matter present, turbidity may have a varying effect on variables such as BGA, fDOM, DO, and SC, thus generating mixed relationships over time.

Overall the application of the developed water quality estimation method in the four selected test cases demonstrated the effectiveness for quantifying and visualizing the spatial trends for a range of variables. This study represents the potential for higher temporal frequency monitoring when utilizing multisensor data such as the HLS product. Implementing these techniques within a cloud computing environment would further expand the practical capabilities by reducing barriers of implementation such as computing resources and data availability. Previous studies have identified issues related to regional transferability, yet as noted in Dörnhöfer and Oppelt (2016) and Schaeffer et al. (2013) water resource managers often prefer regionally developed models as they can produce estimations with actionable accuracies when compared to analytical/global models. Incorporating time series analysis and anomaly detection into workflows such as these, a better understanding of complex inland water dynamics such as the development harmful algal blooms may be achieved. The use of an automated, cloud-based system, employing the techniques defined in this study could lead to the development of an automated anomaly detection and monitoring system that would further enable water resource managers and researchers to combat and respond to water quality issues.

5. Conclusions

Using Landsat-8 and Sentinel-2 data a harmonized (HLS) dataset was produced within a cloud computing environment. Combining the data from these sensors significantly increased the temporal frequency which is required for dynamic systems such as inland water bodies. In this study, a novel deep learning architecture (pDNN) was established and tested proving to have robust

estimation accuracy across a range of variables. The results from this study further showed that the pDNN approach significantly outperformed MLR, SVR, and ELR in terms of overall accuracy and error. Applying the developed pDNN method to all available HLS data for the four locations time series of estimated water quality variables were accurately produced. Initial results indicate that the pDNN method is suitable for regional scale implementations given the hydrologic conditions across the study area. Using the EDA anomaly detection technique irregular water quality events were identified and analyzed. The results from the anomaly detection and time series analysis showed distinct relationships between variables and an apparent trend in seasonality especially for BGA which supports previous findings. Levels of SC were also estimated at a high accuracy and were shown to be highly correlated to concentrations of Chl and fDOM, proving that indirect estimation may serve as an approach for modeling non-optical variables. Furthermore, applying the developed methods to the HLS imagery displayed relatively high-resolution spatial distributions and trends in water quality. The results from this study suggest that a regional water quality estimation and anomaly detection system built on cloud computing and deep learning algorithms could be ideal for areas of key interest and provide the framework for low cost accurate systems.

Research Highlights

- Virtual constellation of Landsat-8 and Sentinel-2 data using google cloud computing
- Established a novel and robust deep learning for water quality estimation
- Estimated a suite of water quality variables with high accuracy
- Anomaly detection for water quality

Acknowledgements

A special thanks to Saint Louis University, National Great Rivers Research and Education Center, and all who assisted in the research. The authors would also like to extend thanks to the reviewers and editor for their thoughtful review and constructive comments.

Disclosure Statement

The authors declare no conflicts of interest.

Funding

This research received no additional funding; National Aeronautics and Space Administration [NNX15AK03H]; National Science Foundation [IIA-1355406; IIA-1430427].

ORCID

Vasit Sagan http://orcid.org/0000-0003-4375-2096
John J. Sloan http://orcid.org/0000-0001-5515-905X

References

Andrews, D. F. 1974. "A Robust Method for Multiple Linear Regression." *Technometrics* 16 (4): 523–531. doi:10.1080/00401706.1974.10489233.

Angelov, P. 2014. "Outside the Box: An Alternative Data Analytics Framework." *Journal of Automation, Mobile Robotics and Intelligent Systems* 8 (2): 53–59.

Angelov, P., and R. Yager. 2011. "A New Type of Simplified Fuzzy Rule-based System." *International Journal of General Systems* 41 (2): 163–185. doi:10.1080/03081079.2011.634807.

Angelov, P. P., X. Gu, J. Principe, and D. Kangin. 2016. "Empirical Data Analysis - A New Tool for Data Analytics". *IEEE International Conference on Systems, Man, and Cybernetics*: 53–59.

Chiang, L. C., Y. Yuan, M. Mehaffey, M. Jackson, and I. Chaubey. 2012. "Assessing SWAT's Performance in the Kaskaskia River Watershed as Influenced by the Number of Calibration Stations Used." *Hydrological Processes* 28 (3): 676–687. doi:10.1002/hyp.9589.

Claverie, M., J. Ju, J. G. Masek, J. L. Dungan, E. F. Vermote, J.-C. Roger, S. V. Skakun, and C. Justice. 2018. "The Harmonized Landsat and Sentinel-2 Surface Reflectance Data Set." *Remote Sensing of Environment* 219: 141–161. doi:10.1016/j.rse.2018.09.002.

Claverie, M., J. G. Masek, J. Ju, and J. L. Dungan. 2017. *Harmonized Landsat-8 Sentinel-2 (HLS) Product User's Guide*. Washington, DC: National Aeronautics and Space Administration (NASA).

Dekker, A. G., T. J. Malthus, and E. Seyhan. 1991. "Quantitative Modeling of Inland Water Quality for High-resolution MSS Systems." *IEEE Transactions on Geoscience and Remote Sensing* 29 (1): 89–95. doi:10.1109/36.103296.

Doerffer, R. 2008. *MERIS Regional Coastal and Lake Case 2 Water Project Atmospheric Correction ATBD*, 21502. Geesthacht, Germany: GKSS Research Center.

Doerffer, R., and H. Schiller. 2007. "The MERIS Case 2 Water Algorithm." *International Journal of Remote Sensing* 28 (3–4): 517–535. doi:10.1080/01431160600821127.

Dörnhöfer, K., and N. Oppelt. 2016. "Remote Sensing for Lake Research and monitoring–Recent Advances." *Ecological Indicators* 64: 105–122. doi:10.1016/j.ecolind.2015.12.009.

Doxoran, D., J. M. Froidefond, and P. Castaing. 2003. "Remote-sensing Reflectance of Turbid Sediment-dominated Waters Reduction of Sediment Type Variations and Changing Illumination Conditions Effects by Use of Reflectance Ratios." *Applied Optics* 42: 2623–2634. doi:10.1364/AO.42.002623.

Duan, W. K., T. B. He, P. Luo, D. Nover, and Y. Yamashiki. 2013. "Spatial and Temporal Trends in Estimates of Nutrient and Suspended Sediment Loads in the Ishikari River Japan." *Science of the Total Environment* 461: 499–508. doi:10.1016/j.scitotenv.2013.05.022.

Gholizadeh, M., A. Melesse, and L. Reddi. 2016. "A Comprehensive Review on Water Quality Parameters Estimation Using Remote Sensing Techniques." *Sensors* 16 (18): 1298. doi:10.3390/s16081298.

Gu, X., and P. Angelov. 2017. "Autonomous Anomaly Detection." In *Evolving and Adaptive Intelligent Systems (EAIS)*, Ljubljana, Slovenia. 1–8. IEEE.

Hornik, K., M. Stinchcombe, and H. White. 1989. "Multilayer Feedforward Networks are Universal Approximators." *Neural Networks* 2 (5): 359–366. doi:10.1016/0893-6080(89)90020-8.

Huang, G. B., Q. Y. Zhu, and C. K. Siew. 2006. "Extreme Learning Machine: Theory and 641 Applications." *Neurocomputing* 70: 489–501. doi:10.1016/j.neucom.2005.12.126.

Kang, E., J. Min, and J. C. Ye. 2017. "A Deep Convolutional Neural Network Using Directional Wavelets for Low-dose X-ray CT Reconstruction." *Medical Physics* 44: 10. doi:10.1002/mp.2017.44.issue-10.

Kohler, C. C., R. J. Sheehan, and J. J. Sweatman. 1993. "Largemouth Bass Hatching Success and First-winter Survival in Two Illinois Reservoirs." *North American Journal of Fisheries Management* 13 (1): 125–133. doi:10.1577/1548-8675(1993)013<0125:LBHSAF>2.3.CO;2.

Kutser, T., B. Paavel, C. Verpoorter, M. Ligi, T. Soomets, K. Toming, and G. Casal. 2016. "Remote Sensing of Black Lakes and Using 810 Nm Reflectance Peak for Retrieving Water Quality Parameters of Optically Complex Waters." *Remote Sensing* 8 (6): 497. doi:10.3390/rs8060497.

Lary, D. J., A. H. Alavi, A. H. Gandomi, and A. L. Walker. 2016. "Machine Learning in Geosciences and Remote Sensing." *Geoscience Frontiers* 7 (1): 3–10. doi:10.1016/j.gsf.2015.07.003.

Lathrop, R. G., and T. M. Lillesand. 1989. "Monitoring Water-quality and River Plume Transport in Green Bay, Lake-Michigan with SPOT-1 Imagery." *Photogrammetric Engineering and Remote Sensing* 55: 349–354.

Li, J., and D. P. Roy. 2017. "A Global Analysis of Sentinel-2A, Sentinel-2B and Landsat-8 Data Revisit Intervals and Implications for Terrestrial Monitoring." *Remote Sensing* 9 (9): 902.

Lim, J., and M. Choi. 2015. "Assessment of Water Quality Based on Landsat 8 Operational Land Imager Associated with Human Activities in Korea." *Environmental Monitoring and Assessment* 187 (6): 384. doi:10.1007/s10661-015-4616-1.

Lipton, Z. C. 2016. "The Mythos of Model Interpretability." *arXiv Preprint arXiv*: 1606.03490.

Louis, J., V. Debaecker, B. Pflug, M. Main-Knorn, J. Bieniarz, U. Mueller-Wilm, E. Cadau, and F. Gascon. 2016. "Sentinel-2 Sen2cor: L2a Processor for Users." Paper presented at the Proceedings of the Living Planet Symposium. Prague, Czech Republic

MacKay, D. J. 1992. "A Practical Bayesian Framework for Backpropagation Networks." *Neural Computation* 4 (3): 448–472. doi:10.1162/neco.1992.4.3.448.

Moonesinghe, H., and P. Tan. 2006. "Outlier Detection Using Random Walks". *Proceedings of the 18th IEEE International Conference on Tools with Artificial Intelligence (ICTAI'06)*. Arlington, VA. 532–539.

Nielsen, M. A. 2015. *Neural Networks and Deep Learning*. Vol. 25. USA: Determination press.

Odermatt, D., A. Gitelson, V. E. Brando, and M. Schaepman. 2012. "Review of Constituent Retrieval in Optically Deep and Complex Waters from Satellite Imagery." *Remote Sensing of Environment* 118: 116–126. doi:10.1016/j.rse.2011.11.013.

Pahlevan, N., S. K. Chittimalli, S. V. Balasubramanian, and V. Vellucci. 2019. "Sentinel-2/Landsat-8 Product Consistency and Implications for Monitoring Aquatic Systems." *Remote Sensing of Environment* 220: 19–29. doi:10.1016/j.rse.2018.10.027.

Pahlevan, N., Z. Lee, J. Wei, C. Schaff, J. Schott, and A. Berk. 2014. "On-orbit Radiometric Characterization of OLI (Landsat-8) for Applications in Aquatic Remote Sensing." *Remote Sensing of Environment* 154: 272–284. doi:10.1016/j.rse.2014.08.001.

Pearce, A. R., L. G. Chambers, and E. A. Hasenmueller. 2017. "Characterizing Nutrient Distributions and Fluxes in a Eutrophic Reservoir, Midwestern United States." *Science of the Total Environment* 581: 589–600. doi:10.1016/j.scitotenv.2016.12.168.

Pellerin, B. A., B. A. Stauffer, D. A. Young, D. J. Sullivan, S. B. Bricker, M. R. Walbridge, A. C. Gerard Jr, and D. M. Shaw. 2016. "Emerging Tools for Continuous Nutrient Monitoring Networks: Sensors Advancing Science and Water Resources Protection." *Journal of the American Water Resources Association (JAWRA)* 52 (4): 993–1008. doi:10.1111/1752-1688.12386.

Pereira, L. S., L. C. Andes, A. L. Cox, and A. Ghulam. 2018. "Measuring Suspended-Sediment Concentration and Turbidity in the Middle Mississippi and Lower Missouri Rivers Using Landsat Data." *JAWRA Journal of the American Water Resources Association* 54 (2): 440–450. doi:10.1111/1752-1688.12616.

Peterson, K., V. Sagan, P. Sidike, A. Cox, and M. Martinez. 2018a. "Suspended Sediment Concentration Estimation from Landsat Imagery along the Lower Missouri and Middle Mississippi Rivers Using an Extreme Learning Machine." *Remote Sensing* 10: 10. doi:10.3390/rs10101503.

Peterson, K., V. Sagan, P. Sidike, E. Hasenmueller, J. Sloan, and J. Knouft. 2018b. "Machine Learning Based Ensemble Prediction of Water Quality Variables Using Feature-level and Decision-level Fusion with Proximal Remote Sensing." *Photogrammetric Engineering and Remote Sensing 85* (4):269–280.

Reavie, E. D., R. P. Barbiero, L. E. Allinger, and G. J. Warren. 2014. "Phytoplankton Trends in the Great Lakes, 2001–2011." *Journal of Great Lakes Research* 40 (3): 618–639. doi:10.1016/j.jglr.2014.04.013.

Ritchie, J. C., P. V. Zimba, and J. H. Everitt. 2003. "Remote Sensing Techniques to Assess Water Quality." *Photogrammetric Engineering & Remote Sensing* 69: 695–704. doi:10.14358/PERS.69.6.695.

Robert, C. 2014. *Machine Learning, a Probabilistic Perspective*. Cambridge, Massachusetts: MIT Press.

Rokni, K., A. Ahmad, K. Solaimani, and S. Hazini. 2015. "A New Approach for Surface Water Change Detection: Integration of Pixel Level Image Fusion and Image Classification Techniques." *International Journal of Applied Earth Observation and Geoinformation* 34: 226–234. doi:10.1016/j.jag.2014.08.014.

Romano, S. P., S. G. Baer, J. J. Zaczek, and K. W. J. Williard. 2009. "Site Modelling Methods for Detecting Hydrologic Alteration of Flood Frequency and Flood Duration in the Floodplain below the Carlyle Dam, Lower Kaskaskia River, Illinois, USA." *River Research and Applications* 25: 975–984. doi:10.1002/rra.1195.

Ryan, K., and K. Ali. 2016. "Application of a Partial Least-squares Regression Model to Retrieve Chlorophyll-a Concentrations

in Coastal Waters Using Hyper-spectral Data." *Ocean Science Journal* 51 (2): 209–221. doi:10.1007/s12601-016-0018-8.

Schaeffer, B. A., K. G. Schaeffer, D. Keith, R. S. Lunetta, R. Conmy, and R. W. Gould. 2013. "Barriers to Adopting Satellite Remote Sensing for Water Quality Management." *International Journal of Remote Sensing* 34 (21): 7534–7544. doi:10.1080/01431161.2013.823524.

Schmidhuber, J. 2015. "Deep Learning in Neural Networks: An Overview." *Neural Networks* 61: 85–117. doi:10.1016/j.neunet.2014.09.003.

Schölkopf, B., and A. J. Smola. "Learning with Kernels: Support Vector Machines, Regularization, Optimization, and Beyond." Accessed 15 October 2018. https://dl.acm.org/citation.cfm?id=559923

Sudheer, K. P., I. Chaubey, and V. Garg. 2006. "Lake Water Quality Assessment from Landsat Thematic Mapper Data Using Neural Network: An Approach to Optimal Band Combination Selection." *Journal of American Water Resources* 42: 1683–1695. doi:10.1111/j.1752-1688.2006.tb06029.x.

Svab, E., A. N. Tyler, T. Preston, M. Presing, and K. V. Balogh. 2005. "Characterizing the Spectral Reflectance of Algae in Lake Waters with High Suspended Sediment Concentrations." *International Journal of Remote Sensing* 26: 919–928. doi:10.1080/0143116042000274087.

Thomas, C., and N. Balakrishnan. 2009. "Improvement in Intrusion Detection with Advances in Sensor Fusion." *IEEE Transactions on Information Forensics and Security* 4 (3): 542–551. doi:10.1109/TIFS.2009.2026954.

Toming, K., T. Kutser, A. Laas, M. Sepp, B. Paavel, and T. Nõges. 2016. "First Experiences in Mapping Lake Water Quality Parameters with Sentinel-2 MSI Imagery." *Remote Sensing* 8: 8. doi:10.3390/rs8080640.

Urbanski, J. A., A. Wochna, I. Bubak, W. Grzybowski, K. Lukawska-Matuszewska, M. Łącka, S. Śliwińska, B. Wojtasiewicz, and M. Zajączkowski. 2016. "Application of Landsat 8 Imagery to Regional-scale Assessment of Lake Water Quality." *International Journal of Applied Earth Observation and Geoinformation* 51: 28–36. doi:10.1016/j.jag.2016.04.004.

Van Der Woerd, H. J., and R. Pasterkamp. 2008. "HYDROPT: A Fast and Flexible Method to Retrieve Chlorophyll-A from Multispectral Satellite Observations of Optically Complex Coastal Waters." *Remote Sensing of Environment* 112 (4): 1795–1807. doi:10.1016/j.rse.2007.09.001.

Vapnik, V. 1995. *The Nature of Statistical Learning Theory*. New York: Springer.

Vermote, E., C. Justice, M. Claverie, and B. Franch. 2016. "Preliminary Analysis of the Performance of the Landsat 8/OLI Land Surface Reflectance Product." *Remote Sensing of Environment* 185: 46–56. doi:10.1016/j.rse.2016.04.008.

Wallace, J., P. Champagne, and G. Hall. 2016. "Time Series Relationships between Chlorophyll-a, Dissolved Oxygen, and pH in Three Facultative Wastewater Stabilization Ponds." *Environmental Science: Water Research & Technology* 2 (6): 1032–1040.

Wang, Z., K. Kawamura, Y. Sakuno, X. Fan, Z. Gong, and J. Lim. 2017. "Retrieval of Chlorophyll-a and Total Suspended Solids Using Iterative Stepwise Elimination Partial Least Squares (ISE-PLS) Regression Based on Field Hyperspectral Measurements in Irrigation Ponds in Higashihiroshima, Japan." *Remote Sensing* 9: 3.

Wilde, F. D., M. W. Sandstrom, and S. C. Skrobialowski. 2014. "Selection of equipment for water sampling (ver. 3.1): US Geological Survey Techniques of Water-Resources Investigations, book 9, chap. A2, 78.[en línea]".

Zhang, L., L. Zhang, and B. Du. 2016. "Deep Learning for Remote Sensing Data: A Technical Tutorial on the State of the Art." *IEEE Geoscience and Remote Sensing Magazine* 4 (2): 22–40. doi:10.1109/MGRS.2016.2540798.

Zhu, X. X., D. Tuia, L. Mou, G. S. Xia, L. Zhang, F. Xu, and F. Fraundorfer. 2017. "Deep Learning in Remote Sensing: A Comprehensive Review and List of Resources." *IEEE Geoscience and Remote Sensing Magazine* 5 (4): 8–36. doi:10.1109/MGRS.2017.2762307.

Zhu, Z., S. Wang, and C. E. Woodcock. 2015. "Improvement and Expansion of the Fmask Algorithm: Cloud, Cloud Shadow, and Snow Detection for Landsats 4–7, 8, and Sentinel 2 Images." *Remote Sensing of Environment* 159: 269–277. doi:10.1016/j.rse.2014.12.014.